ISME

www.nature.com/ismej

ARTICLE

Light-independent anaerobic microbial oxidation of manganese driven by an electrosyntrophic coculture

Lingyan Huang[1,2,4], Xing Liu[2,4], Christopher Rensing[2], Yong Yuan[1✉], Shungui Zhou[2] and Kenneth H. Nealson[3]

Anaerobic microbial manganese oxidation (AMMO) has been considered an ancient biological metabolism for Mn element cycling on Archaean Earth before the presence of oxygen. A light-dependent AMMO was recently observed under strictly anoxic conditions, providing a new proxy for the interpretation of the evolution of oxygenic photosynthesis. However, the feasibility of biotic Mn(II) oxidation in dark geological habitats that must have been abundant remains unknown. Therefore, we discovered that it would be possible to achieve AMMO in a light-independent electrosyntrophic coculture between *Rhodopseudomonas palustris* and *Geobacter metallireducens*. Transmission electron microscopy analysis revealed insoluble particle formation in the coculture with Mn(II) addition. X-ray diffraction and X-ray photoelectron spectroscopy analysis verified that these particles were a mixture of MnO_2 and Mn_3O_4. The absence of Mn oxides in either of the monocultures indicated that the Mn(II)-oxidizing activity was induced via electrosyntrophic interactions. Radical quenching and isotopic experiments demonstrated that hydroxyl radicals (•OH) produced from H_2O dissociation by *R. palustris* in the coculture contributed to Mn(II) oxidation. All these findings suggest a new, symbiosis-dependent and light-independent AMMO route, with potential importance to the evolution of oxygenic photosynthesis and the biogeochemical cycling of manganese on Archaean and modern Earth.

The ISME Journal (2023) 17:163–171; https://doi.org/10.1038/s41396-022-01335-3

INTRODUCTION

Microbial Mn(II) oxidation (MMO) is an important biogeochemical process in the global cycles of various trace metals and nutrients because of the remarkable oxidation and adsorption properties of the generated Mn(III/IV) oxides [1–3]. Previous studies have shown that MMO could primarily be attributed to direct enzymatic oxidation by multicopper oxidases or heme peroxidases in bacteria such as *Bacillus* spp. and *Erythrobacter* sp. [4, 5], or indirectly by biogenic reactive oxygen species (e.g., superoxide radical (O_2^{-}•)) in some species, such as *Stilbella aciculosa* and *Roseobacter* sp. [6, 7]. All these MMO processes require substantial free oxygen concentrations. Even the new group of manganese oxidizers reported by Yu et al., which accomplish Mn(II) oxidation syntrophically, require oxygen to drive the formation of manganese oxides [8]. In addition to aerobic MMO, an anaerobic MMO (AMMO) process in the absence of oxygen, relevant for Archaean Earth, has also drawn great attention in recent years because Mn oxides in ancient environments have been used as an important geochemical signal for the evolution of oxygenic photosynthesis prior to the Great Oxidation Event (GOE) [9–11]. However, the occurrence and mechanism of Mn(II) oxidation in the absence of oxygen on Archaean Earth remain poorly understood.

Light seems necessary for anaerobic manganese oxidation. As reported by Liu et al., rhodochrosite ($MnCO_3$), an Archean manganese mineral, can be photochemically oxidized into manganite (γ-MnOOH) by UV light under anoxic and abiotic conditions, providing an alternative mechanism for producing manganese oxides in the absence of molecular oxygen [12]. In yet another variation, Daye et al. incubated anoxygenic photosynthetic biofilm from a meromictic lake, and reported that these photosynthetic biofilms could anaerobically oxidize Mn(II) under light illumination [13]. They demonstrated that this AMMO relied on the light-dependent interaction between the anoxygenic photosynthetic microorganism *Chlorobium* sp. and *Geobacter* species via interspecies electron transfer (IET). This finding provides some new possibilities for the interpretation of the evolution of oxygenic photosynthesis and the role of microbial syntrophy in that evolution and in biogeochemical Mn cycling on the early Earth. However, many geological environments (e.g., nearly all marine and freshwater sediments) have anoxic dark zones, even on modern Earth; therefore, it is of great interest to know the feasibility of Mn(II) oxidation in these dark and anoxic environments.

IET is a process of syntrophic electron exchange between two microorganisms using mediators or direct contact, which has been shown to endow microorganisms with unexpected abilities such as methane oxidation, carbon fixation, and bioremediation of contaminants [14–16]. IET has been described in several model microbial cocultures, including *Geobacter metallireducens* and *Geobacter sulfurreducens* [17], *G. metallireducens* and *Methanosarcina barkeri* [18], and *Syntrophomonas wolfei* and *Methanobacterium*

[1]Guangdong Key Laboratory of Environmental Catalysis and Health Risk Control, School of Environmental Science and Engineering, Institute of Environmental Health and Pollution Control, Guangdong University of Technology, Guangzhou, China. [2]Fujian Provincial Key Laboratory of Soil Environmental Health and Regulation, College of Resources and Environment, Fujian Agriculture and Forestry University, Fuzhou, China. [3]Department of Earth Science, University of Southern California, Los Angeles, CA, USA. [4]These authors contributed equally: Lingyan Huang, Xing Liu. ✉email: yuanyong@soil.gd.cn

Received: 12 May 2022 Revised: 8 October 2022 Accepted: 11 October 2022
Published online: 19 October 2022

formicicum [19]. A novel light-independent electrosyntrophic interaction was recently observed in *Rhodopseudomonas palustris*, a well-known anoxygenic photosynthetic bacterium [20], and *G. metallireducens* coculture under dark and anoxic conditions, which revealed a new metabolic form, i.e., syntrophic electroautotrophy, for anoxygenic phototrophs [21]. This unique electrosyntrophic coculture was shown to contribute to dark CO_2 fixation. Inspired by previous evidence of Mn(II) oxidation driven by anoxygenic photosynthetic microorganisms [13, 22], a variation in the Mn(II) oxidation process was expected in this electrosyntrophic coculture. In particular, the report of Daye et al. [13] stimulated us to examine the possibility of a syntrophically driven light-independent AMMO, analogous to the abovementioned anaerobic light-independent symbioses [21].

In this study, we provide experimental evidence that the electrosyntrophic interaction between *R. palustris* and *G. metallireducens* can catalyze AMMO under anoxic dark conditions, and we show that this light-independent IET results in Mn(II) oxidation to Mn(III/IV) oxides under strictly anoxic conditions. By electrochemical and radical quenching tests, the significant role of •OH in this AMMO was confirmed. The results of this study provide a mechanism whereby ancient anoxygenic photosynthesis could have been involved in the production of Mn(III/IV) oxides in a more diverse pathway, offering new data that should be considered when discussing the evolution of oxygenic photosynthesis and biogeochemical Mn cycling on Earth.

MATERIALS AND METHODS

Microorganisms and culture medium

G. metallireducens GS15 and *R. palustris* CGMCC 1.2180 were both obtained from frozen stocks in our laboratory and were initially purchased from the Deutsche Sammlung von Mikroorganismen und Zellkulturen and the China General Microbiological Culture Collection Center, respectively. Pure cultures of *G. metallireducens* and *R. palustris* were anaerobically grown at 30 °C in FCA and 0259 medium, respectively [21]. *R. palustris* was incubated under illumination with an LED light (15 W, with an optical power density of 20 Wm^{-2}) as previously described [23]. Coculture of *G. metallireducens* and *R. palustris* was anaerobically cultured at 30 °C in nutrient broth (NB) medium in the dark, with 20 mM acetate as the electron donor and 30 mM nitrate as the electron acceptor [21]. The culture medium was aerated with mixed gas (N_2:CO_2, 80:20) to remove oxygen and then sterilized using an autoclave. The cocultures were transferred at least six times to obtain a stable electrosyntrophic interaction between *G. metallireducens* and *R. palustris* [24]. For AMMO experiments, Mn(II) was added as $MnCl_2$ to a final concentration of 1 mM.

Analytical techniques

Acetate oxidation by *G. metallireducens* and *R. palustris* coculture was monitored using ultrahigh-performance liquid chromatography (U3000, Thermo Fisher Scientific, USA) equipped with an Aminex HPX-87H column (Bio-Rad, USA) [25]. Nitrate reduction by the coculture was measured with an ion chromatograph (ICS900, Thermo Fisher Scientific, USA) [26]. The concentration of O_2 in the coculture system was measured using a Neofox-kit-probe (Ocean Optics, USA). First, coculture cells were inoculated into anaerobic blue cap bottles and cultured in an anaerobic glove box at 30 °C. Then, the Neofox-Kit probe was crossed through a rubber plug of the blue cap bottle, and the oxygen concentration was detected. The expression of genes encoding proteins involved in AMMO was analyzed according to transcriptomic data [21].

Characterization of manganese oxides

Mn(III/IV) oxides were detected using the colorimetric reagent Leucoberbelin Blue I (LBB) (SIGMA) as previously described [27]. For measurement, 2 mL samples were mixed vigorously with 1 mL LBB reagent and then poured into the cuvette to monitor the absorbance at 620 nm using a UV/Vis spectrophotometer (UV2600, Shunyuhengping, China). The Mn(III/IV) content was calculated according to the standard curve prepared with $KMnO_4$ solution. Because the LBB assay cannot distinguish Mn(IV) from Mn(III) and Mn(III) would be disproportionate immediately to Mn(II) and Mn(IV), all the determined Mn(III/IV) values were calculated to be Mn(IV) [27]. The high-resolution transmission electron microscopy (TEM) images and selected area electron diffraction (SAED) were analyzed using a field-emission transmission electron microscope (2100F, JEM, Japan). Elemental mapping was performed by an XMaxN energy-dispersive X-ray spectrometer (EDS) attached to the TEM instrument and by scanning electron microscope (SEM, Hitachi SU8010) equipped with an IXRF system. The X-ray diffraction (XRD) patterns were obtained utilizing an X-ray diffractometer (XRD-6000, Shimadzu, Japan). X-ray photoelectron spectroscopy (XPS) experiments were performed using an XPS spectrometer system (Escalab 250XI, Thermo, USA).

Reactive oxygen species (ROS) measurements

The O_2^{-}• concentration was monitored by adding 50 μM nitro blue tetrazolium (NBT) to the culture, and the absorbance at 560 nm was recorded using a UV/Vis spectrometer (UV2600, Shimadzu, Japan) [28, 29]. The concentration of H_2O_2 was determined by using a fluorescence spectrometer (G9800A, Agilent Technologies, USA) to detect the fluorescence at $\lambda_{ex} = 316.5$ nm and $\lambda_{em} = 408.5$ nm formed by H_2O_2 and p-hydroxyphenylacetic acid [30]. The •OH concentration was monitored by adding 0.5 mM purified terephthalic acid and detecting the fluorescence at $\lambda_{ex} = 320$ nm and $\lambda_{em} = 425$ nm using a fluorescence spectrometer (G9800A, Agilent Technologies, USA) [31]. Triplicate measurements were conducted to reproduce the results. The presence of •OH was further verified using electron paramagnetic resonance spectroscopy (EPR) (A300-10/12, Bruker, Germany) with 5,5-dimethyl-1-pyrroline-N-oxide (DMPO) as a trapping agent. For quenching experiments, dimethyl sulfoxide (DMSO, 1 mM), catalase (10 mg/L), and superoxide dismutase (SOD, 10 mg/L) were added to the coculture to quench •OH, H_2O_2, and O_2^{-}•, respectively [7, 28].

Two-chamber microbial fuel cells (MFCs)

H-type cells were employed to construct two-chamber microbial fuel cells (MFCs) as previously described [21, 32]. Briefly, each chamber of the cell had a 25 mL liquid volume and a 5 mL headspace volume. Graphite plates (1.5 × 1.0 × 0.5 cm) were used as the anodic and cathodic electrodes, respectively. A proton exchange membrane (Nafion 117, DuPont, USA) was used to separate the anodic and cathodic chambers. An external resistance (1 MΩ) was applied to connect the anode and cathode, and the voltage across the resistance was recorded using a data acquisition system (Model 2700, Keithley Instruments, USA). NB medium was used as the electrolyte. To initiate the two-chamber MFCs, 1 mL of *G. metallireducens* and *R. palustris* cells were inoculated into the anodic and cathodic chambers, respectively. The two-chamber MFCs were wrapped with aluminum foil to maintain darkness and then anaerobically incubated at 30 °C.

Stable isotope analysis

To verify the origin of •OH, ^{18}O-labeled H_2O (SIGMA) was used to replace the normal water for the preparation of the coculture medium. When *G. metallireducens* and *R. palustris* cocultures in the medium grew to their stable phase under dark and anoxic conditions, 80 mM DMPO was added to trap the •OH produced by the cocultures, and then the supernatant was collected and injected into an ultrahigh-performance liquid chromatography-triple quadrupole mass spectrometer (LC–MS, TSQ Endura, Thermo Fisher, USA) for the analysis of DMPO-^{18}OH produced from the reaction of DMPO with •^{18}OH. LC was performed with a Phenomenex C-18 reversed-phase column and detected at 254 nm by a UV detector, and MS was performed in positive ion mode as described previously [33].

RESULTS

Light-independent anaerobic manganese oxidation in *Geobacter* and *Rhodopseudomonas* cocultures

An anoxygenic photosynthetic bacterium (*R. palustris*) formed an electrosyntrophic coculture with *G. metallireducens* under dark and anoxic conditions with acetate as the electron donor and nitrate as the electron acceptor. Metabolism analysis showed that acetate and nitrate were simultaneously metabolized in the coculture (Fig. S1A), supporting a syntrophic interaction between *G. metallireducens* and *R. palustris*. When the coculture was incubated with 1 mM Mn(II) addition, both acetate and nitrate were consumed with time as well (Fig. S1B), and the consumption rates of these compounds were the same as that without Mn

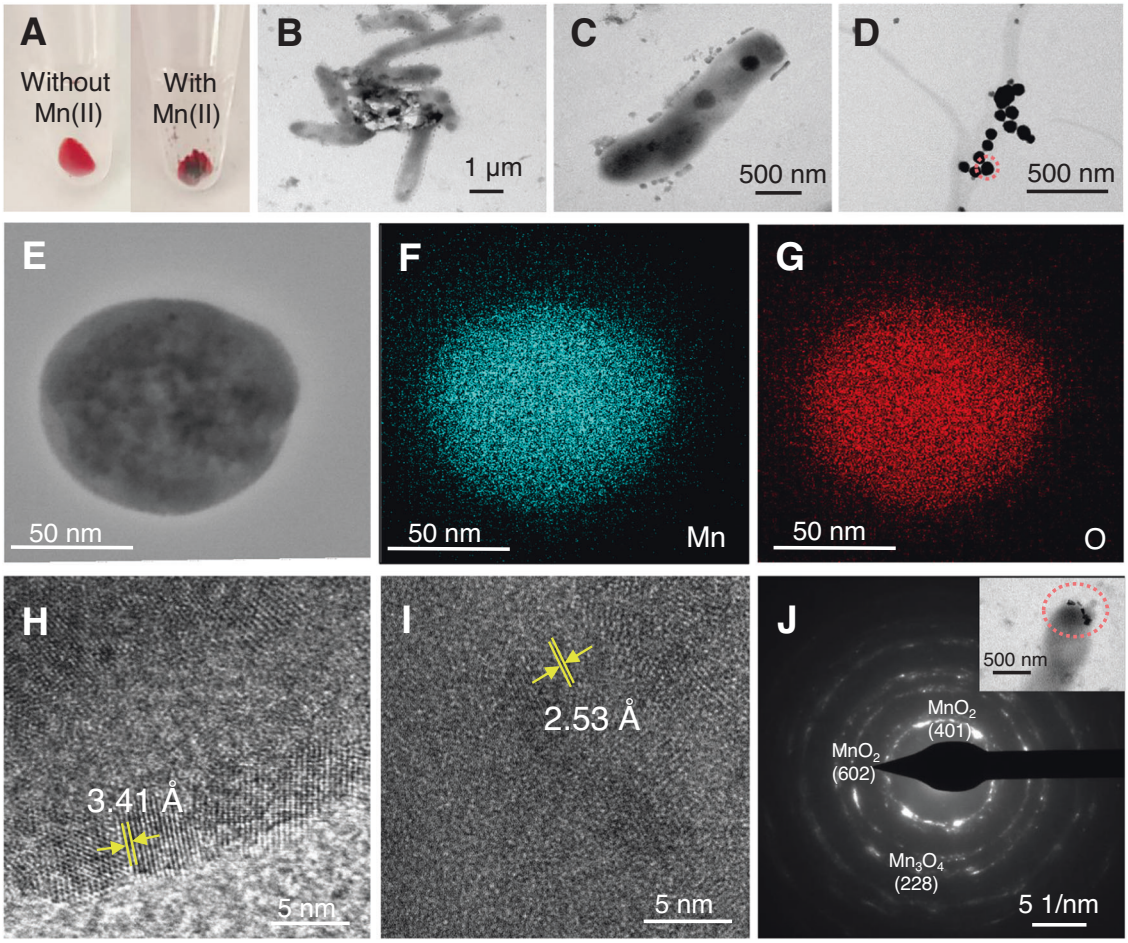

Fig. 1 Manganese oxide formation in electrosyntrophic cocultures of *G. metallireducens* and *R. palustris*. **A** Appearance of cocultures added with or without $MnCl_2$ and incubated under dark anoxic conditions. **B** TEM of *G. metallireducens* and *R. palustris* coculture cells incubated with 1 mM $MnCl_2$. Inner insoluble particles indicated the formation of insoluble manganese oxides. **C** Manganese oxide formation on the surface of coculture cells and **D** around nanowires pictured by high-resolution transmission electron microscope. **E** TEM high-angle annular dark-field image of manganese oxides formed in the coculture marked in **D**. **F** Elemental mappings of Mn and **G** O elements. **H** TEM lattice fringe images of manganese oxides formed in cocultures with d-spacings of 3.41 Å Mn_3O_4 and **I** 2.53 Å MnO_2. **J** SAED patterns of the manganese oxides. The inner picture shows the area selected for SAED analysis.

addition, suggesting that the addition of Mn did not affect the growth of this coculture. Moreover, the color of the coculture turned dark, and some insoluble particles gradually formed (Fig. 1A). These particles were distributed inside the aggregates as well as on the surface of cells and their cellular nanowires (Fig. 1B–D). In contrast, no particles formed in cocultures without the addition of Mn(II) or in heat-killed cocultures after supplying Mn(II) (Fig. S2). Therefore, insoluble Mn oxides were hypothesized to be formed by the coculture. Mn(IV) gradually accumulated in the coculture (Fig. S1C), which was well associated with the growth of the coculture (Fig. S1B), suggesting the dependence of AMMO on the growth of the coculture. The accumulation of Mn(IV) in cocultures reached to 10.39 ± 0.82 μM after incubation for 12 days (Fig. S1C). The single species alone could not grow in the presence or absence of Mn(II) (Fig. S3), which indicated that the electrosyntrophy between *G. metallireducens* and *R. palustris* induced the formation of Mn oxides.

To characterize these Mn oxide particles in more detail, further analyses, including SEM, TEM, and SAED analysis, were performed. The SEM- and TEM-EDS mappings showed that these particles mainly consisted of Mn and O elements (Figs. 1E–G and S4). TEM lattice fringe images showed that these particles had a uniform lattice fringe with interplanar spacing of 3.41 Å and 2.53 Å (Fig. 1H, I), which was consistent with the characteristic value for Mn_3O_4 and MnO_2 [34, 35], respectively. The SAED pattern of these particles also exhibited Bragg diffraction rings for Mn_3O_4 and MnO_2 (Fig. 1J). The composition of these Mn(III/IV) oxides was further investigated by performing XRD and XPS analysis as previously described [30, 36]. The diffraction peaks of the XRD patterns were in agreement with PDF#12-0713 and PDF#03-1041 (Fig. 2A), confirming the formation of both MnO_2 and Mn_3O_4. No diffraction peaks of Mn(III/IV) oxides were observed from the coculture without the addition of Mn(II) (Fig. 2A), excluding the generation of Mn(III/IV) oxides from the culture medium. XPS analysis displayed peaks at 653.9, 642.4, and 83.44 eV (Fig. 2B), which have been reported to be the characteristic peaks of Mn $2p_{1/2}$, Mn $2p_{3/2}$, and Mn 3s [36, 37], respectively. Further measurement of Mn 2p multiplet splitting showed that they were well fitted to MnO_2 and Mn_3O_4 (Fig. 2C). Moreover, the peak splitting of Mn $2p_{1/2}$ and Mn $2p_{3/2}$ is 11.82 eV, which is between the range of 11.3 eV for Mn_3O_4 and 11.9 eV for MnO_2 [30, 38], therefore also indicating the presence of a mixture of MnO_2 and Mn_3O_4. According to previous reports, the peak splitting of Mn 3s is more important for assessing its oxidation state, and the proposed values for MnO_2 and Mn_3O_4 are 4.5 and 5.3 eV, respectively [30, 39]. For our samples, the peak splitting was 5.27 eV (Fig. 2D), which was in the range of 4.5–5.3 eV, implying the shift of Mn(II) to Mn(III/IV). In addition, the XPS survey spectrum had a peak at 5.63 eV on Mn 3p (Fig. S5), which has been proposed to be attributed to Mn_3O_4 [36]. All of these

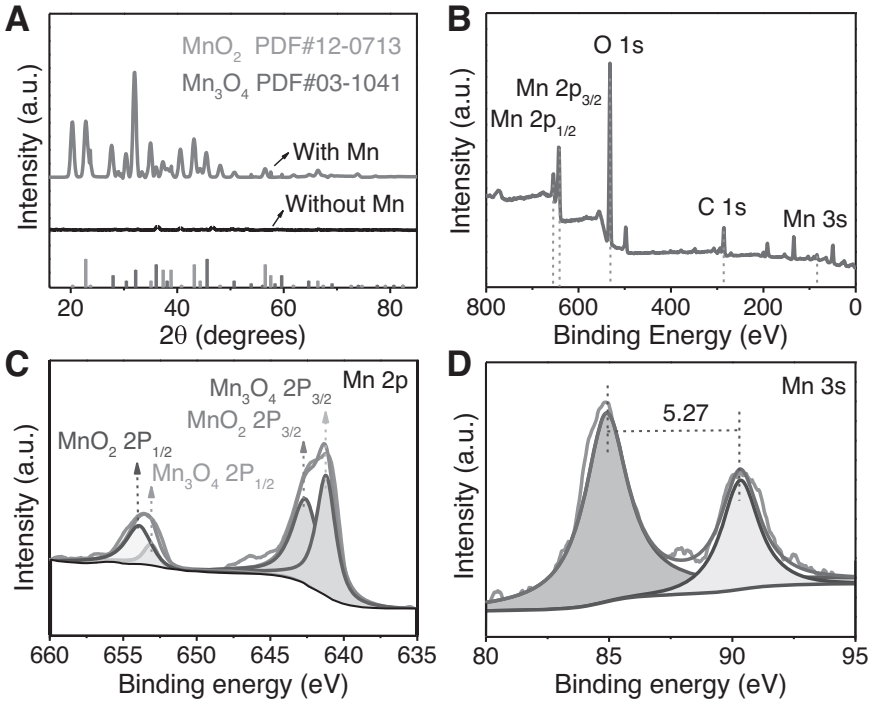

Fig. 2 Characteristics of insoluble manganese oxides. A Smoothed XRD spectra of manganese oxides in the range of $15 \le 2\theta \le 85$. **B** XPS survey spectrum of manganese oxides. **C** XPS analysis of the 2p and **D** 3s spectral regions of manganese oxides.

results revealed that the formed Mn oxides in the coculture were mainly composed of MnO_2 and Mn_3O_4.

Hydroxyl radicals were responsible for anaerobic manganese oxidation in cocultures

MMO has previously been proposed to be catalyzed by Mn oxidases, ROS or high-potential photosynthetic reaction centers under oxic conditions [4, 7, 13]. *G. metallireducens* and *R. palustris* do not possess high-potential photosynthetic reaction centers under dark conditions [40]. Therefore, the possibility of Mn(II) oxidation catalyzed by intrinsic Mn oxidases or ROS was probed. The expression of Mn oxidases, including manganese peroxidases, multicopper oxidases, and heme peroxidases, was analyzed. Genes encoding enzymes potentially catalyzing Mn(II) oxidation, such as multicopper oxidases in *G. metallireducens* and copper oxidases in *R. palustris*, were both expressed at low levels in this coculture (Tables S1a, S2a), excluding the possibility that syntrophic interactions stimulate the expression of silent Mn(II)-oxidizing genes [41]. Taken together, these findings indicated that Mn oxidases should not be involved in AMMO in the *G. metallireducens* and *R. palustris* coculture.

Mn oxidation is very slow in natural environments below pH 9.0 even under oxic conditions due to the high redox potential of Mn (Fig. 3A) [42, 43]. Specifically, the redox potential of the O_2/H_2O couple ($E^0 = 1.23$ V) is slightly lower than that of Mn, therefore the spontaneous abiotic oxidation of Mn(II) is very slow. The oxidation of Mn(II) always requires a catalyst to enhance the oxidation rate by orders of magnitude [44]. In addition to Mn oxidases, ROS, including O_2^{-}•, H_2O_2, and •OH, are considered to be active for Mn oxidation. The E^0 of the O_2^{-}•/H_2O couple is 2.40 V (Fig. 3A), which is higher than that of Mn(II)/Mn(III) but slightly lower than that of Mn(II)/Mn(IV), leading to the fast formation of Mn(III) but a low rate of Mn(IV) formation [45]. The E^0 of H_2O_2/H_2O is 1.76 V, which is far lower than that of O_2^{-}•/H_2O and that of Mn(II)/Mn(IV), exhibiting undesirable oxidation to form Mn(IV) oxides [46]. For the •OH/H_2O couple, E^0 is 2.8 V, which is much higher than that of Mn(II)/Mn(IV), suggesting the chemical feasibility of Mn(II) oxidation into Mn(III/IV) oxides [47]. In view of the above, ROS-mediated Mn(II) oxidation in cocultures was further evaluated in detail. There was no detectable O_2^{-}• in the *G. metallireducens* and *R. palustris* cocultures in the presence or absence of Mn(II) (Fig. 3B). The undetectable O_2^{-}• could have been attributed to its fast consumption. Furthermore, SOD was also added to the system to quench the potential O_2^{-}•. The generation of Mn(III/IV) oxides was not affected (10.37 ± 0.62 μM) in the presence of SOD, thereby eliminating O_2^{-}•-mediated Mn(II) oxidation. Other ROS were further analyzed, showing the presence of •OH and H_2O_2 in the coculture in both the presence and absence of Mn(II) (Fig. 3C, D). The production of •OH was also confirmed using an EPR spectrometer (Fig. 4A). The concentrations of H_2O_2 and •OH increased with the growth of the coculture cells, with maximum concentrations of 89.68 ± 0.52 and 0.83 ± 0.04 μM (Fig. 3E), respectively, indicating that H_2O_2 or •OH may have been involved in AMMO in this coculture. A small amount of Fe(II) existed in the coculture medium, and the accumulation of H_2O_2 was slightly lower in cocultures in the presence of Mn(II) than in the absence of Mn(II) (Fig. 3D), indicating a Mn(II) oxidation reaction by H_2O_2 as follows [45, 48, 49]:

$$Mn^{2+} + H_2O_2 \rightarrow Mn^{3+} + \bullet OH + OH^{-} \quad (1)$$

$$2Mn^{3+} + 2H_2O \rightarrow MnO_2 + Mn^{2+} + 4H^{+} \quad (2)$$

However, the Fenton reaction seems to be only partially responsible for Mn(II) oxidation since the consumed H_2O_2 (4.72 ± 0.13 μM) cannot account for the high Mn(III/IV) production (10.39 ± 0.82 μM). Furthermore, when a H_2O_2 scavenger was added into the coculture, both the oxidation of Mn(II) and the growth of coculture cells remained almost unaffected (Figs. S6, S7A, B), implying a minor role of H_2O_2 on the light-independent AMMO. In contrast, when a •OH scavenger (DMSO) was added to the coculture, the growth of the coculture was almost unaffected (Fig. S7A, B), but the generation of •OH and Mn(II) oxidation was

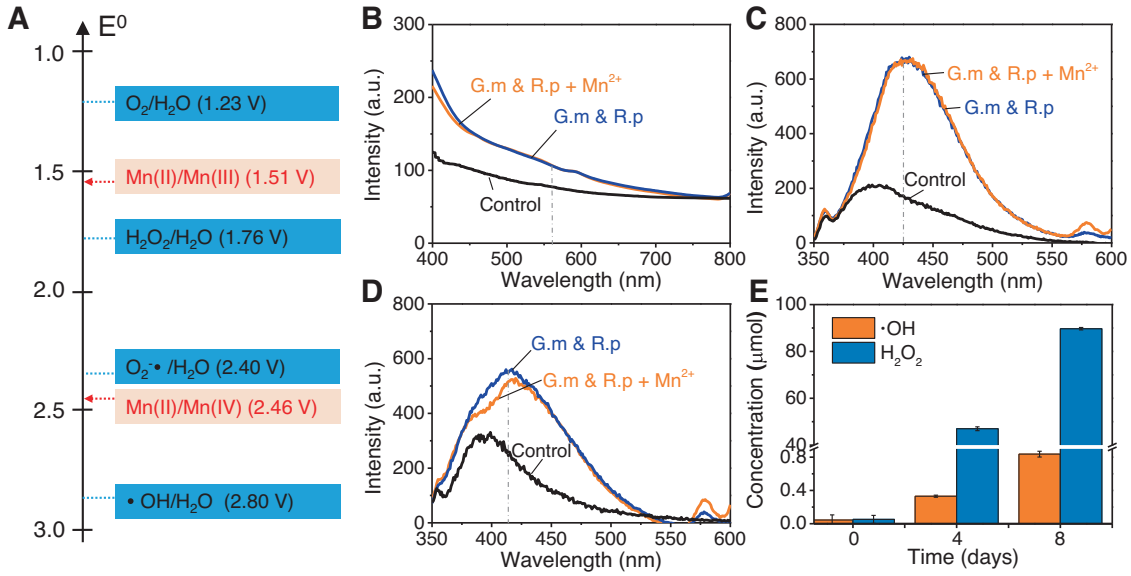

Fig. 3 ROS generation in *G. metallireducens* and *R. palustris* cocultures. A The standard redox potential (E^0) for manganese and reactive oxygenic species, including O_2^-•, H_2O_2, and •OH. **B** UV/Vis spectra detection of O_2^-• in *G. metallireducens* and *R. palustris* cocultures. **C** Fluorescence analysis of •OH and **D** H_2O_2 in this cocultures. **E** •OH and H_2O_2 accumulation in this cocultures.

completely inhibited (Figs. S6A, S7C). Taken together, these results confirmed that both •OH and H_2O_2 produced in the coculture contributed to the AMMO, but •OH was the main contributor. The potential Mn(II) oxidation reaction driven by •OH was as follows [49–51]:

$$Mn^{2+} + \bullet OH \rightarrow Mn^{3+} + OH^- \quad (3)$$

$$2Mn^{3+} + 2H_2O \rightarrow MnO_2 + Mn^{2+} + 4H^+ \quad (4)$$

Hydroxyl radicals were produced during the extracellular electron uptake process of *R. palustris*

To verify the origin of •OH in this coculture, *G. metallireducens* and *R. palustris* were separately incubated in an anodic and a cathodic compartment of two-chamber MFCs under dark and anoxic conditions, respectively (Fig. S8). In the two-chamber MFCs, *G. metallireducens* and *R. palustris* were physically separated by a proton exchange membrane, which would stop the mixture of electrolyte in the anodic and cathodic chambers and help to identify the source of •OH generation. Neither •OH nor H_2O_2 was produced in the compartment containing *G. metallireducens*, while both H_2O_2 and •OH were detectable in the compartment containing *R. palustris* (Fig. S9). In addition, the LBB assays confirmed that Mn(II) cannot be oxidized in the compartment containing *G. metallireducens* but can be oxidized in the compartment containing *R. palustris* (7.31 ± 0.53 μM Mn(IV)). To determine whether •OH generation has existed commonly in electrosyntrophy, another well-studied electrosyntrophic coculture of *G. metallireducens* and *G. sulfurreducens* was explored. Neither Mn oxidation nor •OH generation was observed in this coculture system (Fig. S10). All these results suggested that •OH generation did not occur in all electrosyntrophic coculture system, and the extracellular electron uptake of *R. palustris* was the key process for •OH generation as well as the subsequent Mn(II) oxidation. ROS production generally requires the involvement of oxygen [52, 53], but the oxygen concentration in coculture was low (ca. 0.25 ± 0.07 μM), which therefore could not be the reason for this high •OH generation (0.83 ± 0.04 μM). H_2O was previously shown to be another source for the generation of •OH [54, 55]. Therefore, to further verify the source of •OH in the coculture, stable isotope analysis was conducted by using ^{18}O-labeled H_2O. Only DMPO/^{16}OH was detected in the coculture when the coculture was incubated in ^{16}O-H_2O (Fig. 4B), while DMPO/^{18}OH was present in the coculture in the presence of ^{18}O-labeled H_2O (Fig. 4C), confirming that •OH in the coculture originated from H_2O dissociation.

DISCUSSION

Generally, Mn(II) oxidation occurs under oxic conditions, and the pathways proposed for Mn(II) oxidation mainly include direct oxidation by Mn oxidases and indirect oxidation by free radicals [3, 8]. Recently, it has been shown that Mn(II) oxidation also occurs under anoxic conditions [13, 56]. Herein, the discovery of light-independent AMMO by the electrosyntrophic coculture of *G. metallireducens* and *R. palustris* revealed a previously undescribed pathway for anaerobic manganese oxidation (AMMO). *G. metallireducens* oxidized acetate to produce electrons that were transferred to the outside of this strain, and then the partner strain *R. palustris* took up these electrons via reverse electron flow through the cyclic photosynthetic apparatus (Fig. 5A) [21]. During this unique electron flow process, H_2O was dissociated to produce •OH that finally contributed to Mn(II) oxidation. Nitrate and acetate were used herein as a representative electron acceptor and donor for the coculture of *G. metallireducens* and *R. palustris*, respectively. A relatively high concentration of nitrate was used to accelerate the anaerobic respiration for ATP generation of this coculture. When the light-independent AMMO cocultures were incubated under a relatively low concentration of nitrate (e.g., 5 NO_3^--N mg/L), the growth of coculture and the light-independent AMMO could still be detected (Fig. S11), indicating the possible occurrence of this light-independent AMMO in the natural environment. As previously reported, •OH can be generated from H_2O under anoxic conditions through a one-electron transfer process via some catalysts such as abiotic FeS_2, in which the surface sulfur vacancies and Fe^{3+} were able to stabilize H_2O adsorption to compensate for the apparent energy barrier of H_2O oxidation to generate •OH [54, 55]. In this regard, the Fe-S clusters in anoxygenic photosynthetic bacteria, such as *R. palustris*, which have a wide range of redox potentials and are capable of binding and activating substrates and mediating one-

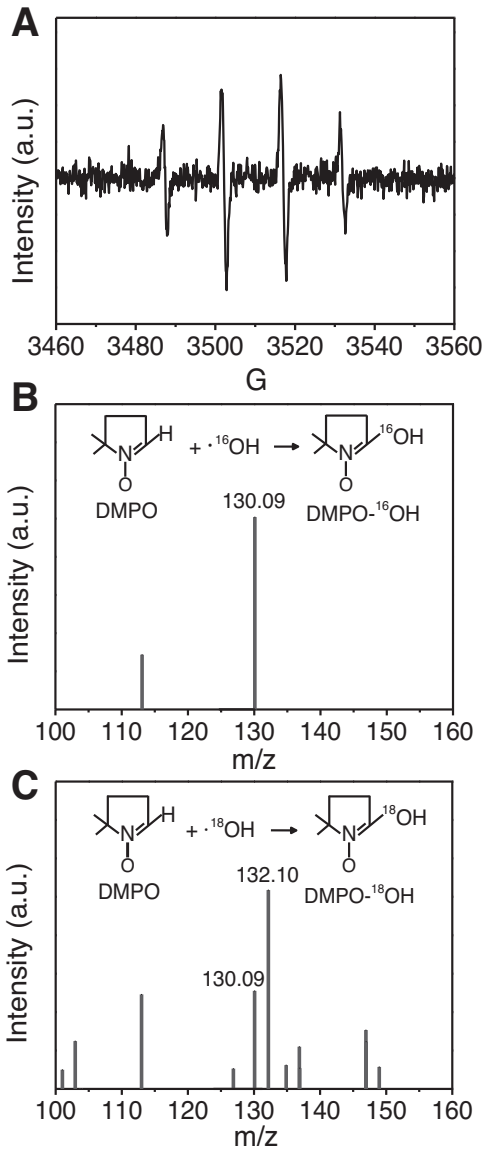

Fig. 4 •OH identification and mass spectra of DMPO/•OH in *G. metallireducens* and *R. palustris* cocultures. A EPR analysis of •OH in *G. metallireducens* and *R. palustris* cocultures. **B** Mass spectra of DMPO/•OH in *G. metallireducens* and *R. palustris* cocultures incubated with ^{16}O-H_2O prepared medium and trapped with DMPO. **C** Mass spectra of DMPO/•OH in *G. metallireducens* and *R. palustris* cocultures cultured with ^{18}O-H_2O prepared medium. The mass-to-charge ratios (m/z) of 130.09 and 132.10 represent DMPO-^{16}OH and DMPO-^{18}OH, respectively.

electron transfer [57–59], are expected to play an important role in the dissociation of H_2O to generate •OH by accepting extracellular electrons from *G. metallireducens* (Fig. 5A). Genes encoding Fe-S proteins in *R. palustris* in coculture were highly expressed (Fig. 5B and Table S1b). Additionally, genes correlated to the SUF system Fe-S cluster assembly proteins that are involved in the biogenesis of Fe-S clusters for photosystems [57, 60], including WP_011158018.1, WP_011158014.1, and WP_011158015.1, were highly expressed in polarized *R. palustris* in the above two-chamber MFCs compared to unpolarized *R. palustris* in an open circuit (Fig. S12). These results suggested that Fe-S clusters of *R. palustris* might participate in •OH generation from H_2O dissociation. Additionally, the transcript level of genes correlated to Fe-S clusters and IET proteins in *G. metallireducens* and *R. palustris* coculture with or without Mn(II) addition was analyzed to verify the possible effect of Mn(II) on the gene expression of this coculture. There were no significant differences in the expression of genes correlated to SUF and IET proteins in cocultures in the presence and absence of Mn(II) (Fig. S13), and the addition of Mn(II) did also not affect the metabolic rate of acetate and nitrate (Fig. S1A, B). These results suggested that Mn(II) oxidation by the coculture was a secondary reaction. Additionally, the Fe-S clusters activated H_2O might also react with the Fe center of cytochrome c to produce •OH [21, 61, 62], which is consistent with the finding that the produced Mn oxides in the coculture were mainly associated with both the cell surface and nanowires where cytochrome c was widely distributed and highly expressed (Fig. 5B and Tables S1c and S2c) [21]. In addition, •OH has been shown to react with organic matter to form H_2O_2 by attacking the carbon centers of organics [63, 64], which would explain the presence of H_2O_2 in this system (Fig. 5A).

The presence of •OH in natural environments, including natural waters, sediments, and soils [65–67], has been widely detected. The •OH generation has been largely considered to be abiotic photochemically driven [68, 69] or aerobic biotic driven reactions [70, 71]. Recent studies have also provided increasing evidence for •OH generation from anoxic waters and sediments [72–74]. However, the mechanism of •OH generation under dark/anoxic conditions remains largely unknown. In this study, •OH was found to be generated from H_2O under anoxic conditions by electro-syntrophic coculture of *G. metallireducens* and *R. palustris*. This phenomenon contradicts the hypothesis that O_2 is needed for ROS generation in biological systems through the univalent reactions of oxygen ($O_2 \rightarrow O_2^{-}\bullet \rightarrow H_2O_2 \rightarrow \bullet OH$) [75–77]. To date, the underlying mechanism of •OH generation from H_2O under anoxic, dark conditions has been proved to be catalyzed by Fe-S clusters, but the exact responsible protein still requires further study.

The occurrence of Mn oxide particles may have been involved in the evolutionary route of oxygenic photosynthesis [78]. However, the formation of early geological Mn oxide particles is still debated. Chernev et al. suggested that Mn oxides might be generated from an anaerobic photosynthesis process by a photosystem II (PS-II) ancestor on early Earth [78]. Daye et al. proposed that Mn oxides are able to be generated in anaerobic photosynthetic biofilms, which was associated with the formation of ordered dolomites that are abundant in ancient rocks but rare in modern ones [11, 13]. In this regard, the formation of Mn oxides from this light-dependent AMMO process may represent a biosignature for past microbial activity in some Archean and Proterozoic [10, 11]. Liu et al. suggested that rhodochrosite, one of the major Archean Mn minerals, could have been photochemically oxidized by light under anoxic, abiotic conditions during the Archean eon [12]. Herein, the finding of light-independent AMMO by the coculture might expand the diversity of Mn redox processes beyond what was thought possible in the presence of high potential photosynthetic reaction centers or light, and offer a new and possible path to explain the formation of Mn(II) oxides on the early Earth.

Mn is mainly present as soluble or adsorbed Mn(II) and insoluble Mn(III/IV) oxides in natural environments [1]. High concentrations of Mn(II) are harmful to human health by causing damage to the nervous system [2, 79]. The oxidation of excess soluble Mn(II) to insoluble and nonbioavailable Mn(III/IV) oxides is an effective strategy to reduce Mn toxicity. The MMO has been mainly detected in aerobic environments because a strong oxidant, such as oxygen, is needed for the oxidation of Mn due to its high redox potential [80]. However, Mn oxides are also present in many anoxic geological environments that are dark, such as marine and freshwater sediments [81, 82]. It is worth mentioning that Mn oxides produced from microbial oxidation generally possess strong oxidation power and large surface area, which are active in attenuating contaminants through adsorption, coprecipitation, and redox reactions in natural environments [83].

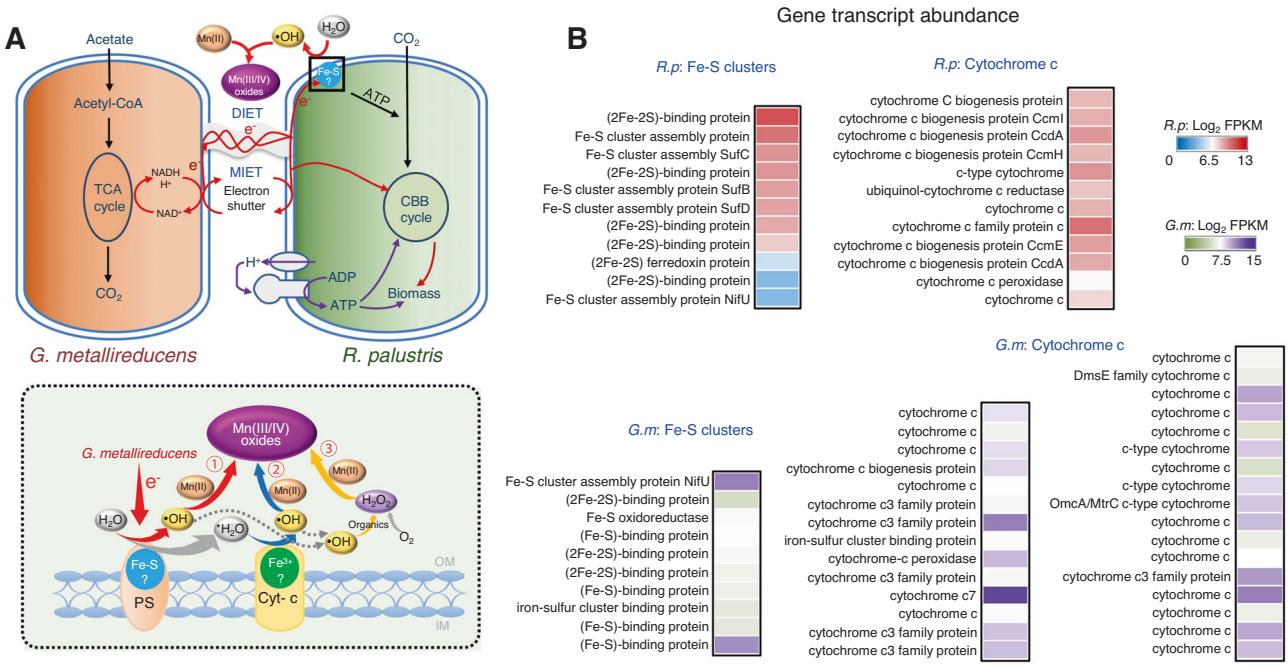

Fig. 5 Strategy of light-independent AMMO in *G. metallireducens* and *R. palustris* cocultures under dark and anoxic conditions. A Putative pathways of the light-independent AMMO by *G. metallireducens* and *R. palustris* coculture. Red lines refer to the electron transfer from *G. metallireducens* to *R. palustris*. The bottom panel displays detailed information of light-independent AMMO for the black dashed square. *H_2O refers to activated H_2O. Fe-S refers to Fe-S clusters. **B** Transcript abundances of related annotated genes in *G. metallireducens* (*G.m*) and *R. palustris* (*R.p*) presented as log_2 FPKM values (fragments per kilobase per million mapped reads) with median log_2 FPKM values of 7.5 and 6.5, respectively. If the log_2 FPKM is larger than the median, it means the gene is highly expressed.

In addition, Mn oxides are able to act as electron acceptors to promote the redox cycles of many other elements, such as C, N, and S, under anoxic conditions [84, 85]. However, less attention has been given to tracing the origin of Mn oxides in anoxic environments. In this regard, the findings of this light-independent AMMO route might also provide a new understanding of Mn cycling and the associated environmental remediation processes in dark, anoxic environments.

CONCLUSION

Our study demonstrates that Mn(II) could be anaerobically oxidized into Mn oxides by the electrosyntrophic coculture of *G. metallireducens* and *R. palustris* under dark conditions. In this Mn(II) oxidation process, *G. metallireducens* oxidizes acetate and transfers extracellular electrons to *R. palustris*, and *R. palustris* accepts the electrons for the dissociation of H_2O to •OH under anoxic conditions. The produced •OH is believed to have catalyzed Mn(II) into Mn oxides. The Fe-S clusters in the photosystem of *R. palustris* were proven to be involved in H_2O dissociation. Different from the previous light-dependent AMMO, the light-independent AMMO here revealed a new AMMO mode under anoxic, dark conditions, suggesting a diverse pathway of microbial Mn metabolism and extending the ecological environment of MMO. All of these findings reveal a new microbial Mn(II) oxidation mode under dark, anoxic conditions, providing a new understanding on the cycling of Mn.

DATA AVAILABILITY

All data are available in the main text or the Supplementary Materials. Additional data related to this paper may be requested from the authors.

REFERENCES

1. Gounot AM. Microbial oxidation and reduction of manganese: consequences in groundwater and applications. FEMS Microbiol Rev. 1994;14:339–49.
2. Roels HA, Bowler RM, Kim Y, Claus HB, Mergler D, Hoet P, et al. Manganese exposure and cognitive deficits: a growing concern for manganese neurotoxicity. Neurotoxicology. 2012;33:872–80.
3. Zhou H, Fu C. Manganese-oxidizing microbes and biogenic manganese oxides: characterization, Mn(II) oxidation mechanism and environmental relevance. Rev Environ Sci Bio. 2020;19:489–507.
4. Butterfield CN, Soldatova AV, Lee SW, Spiro TG, Tebo BM. Mn(II, III) oxidation and MnO_2 mineralization by an expressed bacterial multicopper oxidase. Proc Natl Acad Sci USA. 2013;110:11731–5.
5. Anderson CR, Johnson HA, Caputo N, Davis RE, Torpey JW, Tebo BM. Mn(II) oxidation is catalyzed by heme peroxidases in *Aurantimonas manganoxydans* strain SI85-9A1 and *Erythrobacter* sp. strain SD-21. Appl Environ Microbiol. 2009;75:4130–8.
6. Hansel CM, Zeiner CA, Santelli CM, Webb SM. Mn(II) oxidation by an ascomycete fungus is linked to superoxide production during asexual reproduction. Proc Natl Acad Sci USA. 2012;109:12621–5.
7. Learman DR, Voelker BM, Vazquez-Rodriguez AI, Hansel CM. Formation of manganese oxides by bacterially generated superoxide. Nat Geosci 2011;4:95–98.
8. Yu H, Leadbetter JR. Bacterial chemolithoautotrophy via manganese oxidation. Nature. 2020;583:453–8.
9. Planavsky NJ, Asael D, Hofmann A, Reinhard CT, Lalonde SV, Knudsen A, et al. Evidence for oxygenic photosynthesis half a billion years before the Great Oxidation Event. Nat Geosci. 2014;7:283–6.
10. Bontognali TRR. Anoxygenic phototrophs and the forgotten art of making dolomite. Geology. 2019;47:591–2.
11. Daye M, Higgins J, Bosak T. Formation of ordered dolomite in anaerobic photosynthetic biofilms. Geology. 2019;47:509–12.
12. Liu W, Hao J, Elzinga EJ, Piotrowiak P, Nanda V, Yee N, et al. Anoxic photogeochemical oxidation of manganese carbonate yields manganese oxide. Proc Natl Acad Sci USA. 2020;117:22698–704.
13. Daye M, Klepac-Ceraj V, Pajusalu M, Rowland S, Farrell-Sherman A, Beukes N, et al. Light-driven anaerobic microbial oxidation of manganese. Nature. 2019;576:311–4.
14. Yang P, Tan GYA, Aslam M, Kim J, Lee PH. Metatranscriptomic evidence for classical and RuBisCO-mediated CO_2 reduction to methane facilitated by direct interspecies electron transfer in a methanogenic system. Sci Rep. 2019;9:4116.
15. Ha PT, Lindemann SR, Shi L, Dohnalkova AC, Fredrickson JK, Madigan MT, et al. Syntrophic anaerobic photosynthesis via direct interspecies electron transfer. Nat Commun. 2017;8:13924.

16. Nagarajan H, Embree M, Rotaru AE, Shrestha PM, Feist AM, Palsson BØ, et al. Characterization and modelling of interspecies electron transfer mechanisms and microbial community dynamics of a syntrophic association. Nat Commun. 2013;4:2809.
17. Summers ZM, Fogarty HE, Leang C, Franks AE, Malvankar NS, Lovley DR. Direct exchange of electrons within aggregates of an evolved syntrophic coculture of anaerobic bacteria. Science. 2010;330:1413–5.
18. Rotaru AE, Shrestha PM, Liu F, Markovaite B, Chen S, Nevin KP, et al. Direct interspecies electron transfer between *Geobacter metallireducens* and *Methanosarcina barkeri*. Appl Environ Microbiol. 2014;80:4599–605.
19. Boone DR, Johnson RL, Liu Y. Diffusion of the interspecies electron carriers H_2 and formate in methanogenic ecosystems and its implications in the measurement of K_m for H_2 or formate uptake. Appl Environ Microbiol. 1989;55:1735–41.
20. Guzman MS, Rengasamy K, Binkley MM, Jones C, Ranaivoarisoa TO, Singh R, et al. Phototrophic extracellular electron uptake is linked to carbon dioxide fixation in the bacterium *Rhodopseudomonas palustris*. Nat Commun. 2019;10:1355.
21. Liu X, Huang L, Rensing C, Ye J, Nealson KH, Zhou S. Syntrophic interspecies electron transfer drives carbon fixation and growth by Rhodopseudomonas palustris under dark, anoxic conditions. Sci Adv. 2021;7:eabh1852.
22. Allen JP, Olson TL, Oyala P, Lee WJ, Tufts AA, Williams JC. Light-driven oxygen production from superoxide by Mn-binding bacterial reaction centers. Proc Natl Acad Sci USA. 2012;109:2314–8.
23. Huang L, Liu X, Zhang Z, Ye J, Rensing C, Zhou S, et al. Light-driven carbon dioxide reduction to methane by *Methanosarcina barkeri* in an electric syntrophic coculture. ISME J. 2022;16:370–7.
24. Huang L, Liu X, Ye Y, Chen M, Zhou S. Evidence for the coexistence of direct and riboflavin-mediated interspecies electron transfer in *Geobacter* coculture. Environ Microbiol. 2020;22:243–54.
25. Liu X, Zhuo S, Rensing C, Zhou S. Syntrophic growth with direct interspecies electron transfer between pili-free *Geobacter* species. ISME J 2018;12:2142–51.
26. Chen M, Zhou XF, Yu YQ, Liu X, Zeng RJ, Zhou SG, et al. Light-driven nitrous oxide production via autotrophic denitrification by self-photosensitized *Thiobacillus denitrificans*. Environ Int 2019;127:353–60.
27. Richardson L, Aguilar C, Nealson K. Manganese oxidation in pH and O_2 microenvironments produced by phytoplankton. Limnol oceanogr 1988;33:352–63.
28. Chen M, Zhou X, Chen X, Cai Q, Zeng RJ, Zhou S. Mechanisms of nitrous oxide emission during photoelectrotrophic denitrification by self-photosensitized *Thiobacillus denitrificans*. Water Res. 2020;172:115501.
29. Choi HS, Kim JW, Cha YN, Kim C. A quantitative nitroblue tetrazolium assay for determining intracellular superoxide anion production in phagocytic cells. J Immunoass Immunochem. 2006;27:31–44.
30. Chen X, Feng Q, Cai Q, Huang S, Yu Y, Zeng RJ, et al. Mn_3O_4 nanozyme coating accelerates nitrate reduction and decreases N_2O emission during photoelectrotrophic denitrification by *Thiobacillus denitrificans*-CdS. Environ Sci Technol. 2020;54:10820–30.
31. Barreto JC, Smith GS, Strobel NH, McQuillin PA, Miller TA. Terephthalic acid: a dosimeter for the detection of hydroxyl radicals in vitro. Life Sci. 1995;56:89–96.
32. Huang L, Liu X, Tang J, Yu L, Zhou S. Electrochemical evidence for direct interspecies electron transfer between *Geobacter sulfurreducens* and *Prosthecochloris aestuarii*. Bioelectrochemistry. 2019;127:21–25.
33. Bonini MG, Miyamoto S, Mascio PD, Augusto O. Production of the carbonate radical anion during xanthine oxidase turnover in the presence of bicarbonate. J Biol Chem. 2004;279:51836–43.
34. Ju W, Jin B, Dong C, Wen Z, Jiang Q. Rice-shaped Fe_2O_3@C@Mn_3O_4 with three-layer core-shell structure as a high-performance anode for lithium-ion batteries. J Electroanal Chem. 2020;861:113942.
35. Wang HY, Li DG, Zhu HL, Qi YX, Li H, Lun N, et al. Mn_3O_4/$Ni(OH)_2$ nanocomposite as an applicable electrode material for pseudocapacitors. Electrochim Acta. 2017;249:155–65.
36. Moses Ezhil Raj A, Victoria SG, Jothy VB, Ravidhas C, Wollschläger J, Suendorf M, et al. XRD and XPS characterization of mixed valence Mn_3O_4 hausmannite thin films prepared by chemical spray pyrolysis technique. Appl Surf Sci. 2010;256:2920–6.
37. Qiu W, Lin Z, Xiao H, Zhang G, Gao H, Feng H, et al. Construction of chemical self-charging zinc ion batteries based on defect coupled nitrogen modulation of zinc manganite vertical graphene arrays. Mater Adv. 2021;2:6694–702.
38. Yao B, Xiao T, Makgae OA, Jie X, Gonzalez-Cortes S, Guan S, et al. Transforming carbon dioxide into jet fuel using an organic combustion-synthesized Fe-Mn-K catalyst. Nat Commun 2020;11:6395.
39. Chigane M, Ishikawa M. Manganese oxide thin film preparation by potentiostatic electrolyses and electrochromism. J Electrochem Soc. 2000;147:6.
40. Fischer WW, Hemp J, Johnson JE. Manganese and the evolution of photosynthesis. Orig Life Evol B. 2015;45:351–7.
41. Liang J, Bai Y, Men Y, Qu J. Microbe-microbe interactions trigger Mn(II)-oxidizing gene expression. ISME J. 2017;11:67–77.
42. Reynard D, Maye S, Peljo P, Chanda V, Girault HH, Gentil S. Vanadium-manganese redox flow battery: study of Mn(III) disproportionation in the oresence of other metallic ions. Chemistry. 2020;26:7250–7.
43. Zhang B, Sun L. Why nature chose the Mn_4CaO_5 cluster as water-splitting catalyst in photosystem II: a new hypothesis for the mechanism of O-O bond formation. Dalton Trans. 2018;47:14381–7.
44. Hansel CM, Francis CA. Coupled photochemical and enzymatic Mn(II) oxidation pathways of a planktonic *Roseobacter*-Like bacterium. Appl Environ Microbiol. 2006;72:3543–9.
45. Learman D, Voelker B, Madden A, Hansel C. Constraints on superoxide mediated formation of manganese oxides. Front Microbiol. 2013;4:262.
46. Du X, Oturan MA, Zhou M, Belkessa N, Su P, Cai J, et al. Nanostructured electrodes for electrocatalytic advanced oxidation processes: from materials preparation to mechanisms understanding and wastewater treatment applications. Appl Catal B-Environ. 2021;296:120332.
47. Wang X, Zhang L. Kinetic study of hydroxyl radical formation in a continuous hydroxyl generation system. RSC Adv. 2018;8:40632–8.
48. Cao W, Jin M, Yang K, Chen B, Xiong M, Li X, et al. Fenton/Fenton-like metal-based nanomaterials combine with oxidase for synergistic tumor therapy. J Nanobiotechnol. 2021;19:325.
49. Benon HJB, Cabelli DE Superoxide and hydroxyl radical chemistry in aqueous solution. Springer Netherlands 1995.
50. Hussain S, Ali SF. Manganese scavenges superoxide and hydroxyl radicals: an in vitro study in rats. Neurosci Lett. 1999;261:21–24.
51. Méndez-Alvarez E, Soto-Otero R, Hermida-Ameijeiras A, López-Martín ME, Labandeira-García JL. Effect of iron and manganese on hydroxyl radical production by 6-hydroxydopamine: mediation of antioxidants. Free Radic Bio Med. 2001;31:986–98.
52. Slimen IB, Najar T, Ghram A, Dabbebi H, Ben Mrad M, Abdrabbah M. Reactive oxygen species, heat stress and oxidative-induced mitochondrial damage: a review. Int J Hyperther. 2014;30:513–23.
53. Turrens JF. Mitochondrial formation of reactive oxygen species. J Physiol. 2003;552:335–44.
54. Siahrostami S, Li GL, Viswanathan V, Nørskov JK. One- or two-electron water oxidation, hydroxyl radical, or H_2O_2 evolution. J Phys Chem Lett. 2017;8:1157–60.
55. Ling C, Liu X, Li M, Wang X, Shi Y, Qi J, et al. Sulphur vacancy derived anaerobic hydroxyl radical generation at the pyrite-water interface: pollutants removal and pyrite self-oxidation behavior. Appl Catal B-Environ. 2021;290:120051.
56. Su JF, Zheng SC, Huang TL, Ma F, Shao SC, Yang SF, et al. Simultaneous removal of Mn(II) and nitrate by the manganese-oxidizing bacterium *Acinetobacter* sp. SZ28 in anaerobic conditions. Geomicrobiol J. 2016;33:586–91.
57. Shen G, Golbeck JH Assembly of the bound iron-sulfur clusters in photosystem I. Springer Netherlands 2006:529-48.
58. Beinert H, Kennedy MC, Stout CD. Aconitase as ironminus signsulfur protein, enzyme, and iron-regulatory protein. Chem Rev 1996;96:2335–74.
59. Jin Z, Heinnickel M, Krebs C, Shen G, Golbeck JH, Bryant DA.Biogenesis of iron-sulfur clusters in photosystem I: holo-NfuA from the cyanobacterium Synechococcus sp. PCC 7002 rapidly and efficiently transfers [4Fe-4S] clusters to apo-PsaC in vitro. J Biol Chem. 2008;283:28426–35.
60. Boyd ES, Thomas KM, Dai Y, Boyd JM, Outten FW. Interplay between oxygen and Fe–S cluster biogenesis: insights from the Suf pathway. Biochemistry. 2014;53:5834–47.
61. Boesen T, Nielsen LP, Schramm A. Pili for nanowires. Nat Microbiol. 2021;6:1347–8.
62. Shi L, Dong H, Reguera G, Beyenal H, Lu A, Liu J, et al. Extracellular electron transfer mechanisms between microorganisms and minerals. Nat Rev Microbiol. 2016;14:651–62.
63. Hullar T, Anastasio C. Yields of hydrogen peroxide from the reaction of hydroxyl radical with organic compounds in solution and ice. Atmos Chem Phys 2011;11:7209.
64. Stemmler K, von Gunten U. OH radical-initiated oxidation of organic compounds in atmospheric water phases: part 1. Reactions of peroxyl radicals derived from 2-butoxyethanol in water. Atmos Environ. 2000;34:4241–52.
65. Yuan C, Chin YP, Weavers LK. Photochemical acetochlor degradation induced by hydroxyl radical in Fe-amended wetland waters: impact of pH and dissolved organic matter. Water Res. 2018;132:52–60.
66. Liao P, Yu K, Lu Y, Wang P, Liang Y, Shi Z. Extensive dark production of hydroxyl radicals from oxygenation of polluted river sediments. Chem Eng J 2019;368:700–9.
67. Wan D, Liu FF, Chen JB, Kappler A, Kuzyakov Y, Liu CQ, et al. Microbial community mediates hydroxyl radical production in soil slurries by iron redox transformation. Water Res. 2022;220:118689.
68. Brezonik PL, Fulkerson-Brekken J. Nitrate-induced photolysis in natural waters: controls on concentrations of hydroxyl radical photo-intermediates by natural scavenging agents. Environ Sci Technol. 1998;32:3004–10.

69. Ou Y, Wu J, Meyer JR, Foston M, Fortner JD, Li W. Photoenhanced oxidation of nC_{60} in water: exploring H_2O_2 and hydroxyl radical based reactions. Chem Eng J. 2019;360:665–72.
70. Aguirre J, Ríos-Momberg M, Hewitt D, Hansberg W. Reactive oxygen species and development in microbial eukaryotes. Trends Microbiol. 2005;13:111–8.
71. Zhang T, Hansel CM, Voelker BM, Lamborg CH. Extensive dark biological production of reactive oxygen species in brackish and freshwater ponds. Environ Sci Technol. 2016;50:2983–93.
72. Page SE, Kling GW, Sander M, Harrold KH, Logan JR, McNeill K, et al. Dark formation of hydroxyl radical in Arctic soil and surface waters. Environ Sci Technol. 2013;47:12860–7.
73. Tong M, Yuan S, Ma S, Jin M, Liu D, Cheng D, et al. Production of abundant hydroxyl radicals from oxygenation of subsurface sediments. Environ Sci Technol. 2016;50:214–21.
74. Schaefer CE, Ho P, Berns E, Werth C. Mechanisms for abiotic dechlorination of trichloroethene by ferrous minerals under oxic and anoxic conditions in natural sediments. Environ Sci Technol. 2018;52:13747–55.
75. Pospíšil P, Arató A, Krieger-Liszkay A, Rutherford AW. Hydroxyl radical generation by photosystem II. Biochemistry. 2004;43:6783–92.
76. Minella M, De Laurentiis E, Maurino V, Minero C, Vione D. Dark production of hydroxyl radicals by aeration of anoxic lake water. Sci Total Environ 2015;527-528:322–7.
77. Wang W, Fan W, Huo M, Zhao H, Lu Y. Hydroxyl radical generation and contaminant removal from water by the collapse of microbubbles under different hydrochemical conditions. Water Air Soil Poll. 2018;229:86.
78. Chernev P, Fischer S, Hoffmann J, Oliver N, Assunção R, Yu B, et al. Light-driven formation of manganese oxide by today's photosystem II supports evolutionarily ancient manganese-oxidizing photosynthesis. Nat Commun. 2020;11:6110.
79. Elsner RJ, Spangler JG. Neurotoxicity of inhaled manganese: public health danger in the shower? Med Hypotheses. 2005;65:607–16.
80. Frantz OO, Hofmann A, Wille M, Spangenberg JE, Bekker A, Poulton SW, et al. Aerobic iron and manganese cycling in a redox-stratified Mesoarchean epicontinental sea. Earth Planet Sci Lett. 2018;500:28–40.
81. Baturin GN The geochemistry of manganese and manganese nodules in the ocean, GN Baturin, Ed. (Springer Netherlands, Dordrecht, 1988), pp. 58-82.
82. Calvert SE, Pedersen TF. Sedimentary geochemistry of manganese; implications for the environment of formation of manganiferous black shales. Econ Geol. 1996;91:36–47.
83. Miyata N, Tani Y, Sakata M, Iwahori K. Microbial manganese oxide formation and interaction with toxic metal ions. J Biosci Bioeng. 2007;104:1–8.
84. Wang Y, Stone AT. Reaction of Mn(III,IV) (hydr)oxides with oxalic acid, glyoxylic acid, phosphonoformic acid, and structurally-related organic compounds. Geochim Cosmochim Acta. 2006;70:4477–90.
85. Lu A, Li Y, Liu F, Liu Y, Ye H, Zhuang Z, et al. The photogeochemical cycle of Mn oxides on the Earth's surface. Mineral Mag. 2021;85:22–38.

ACKNOWLEDGEMENTS

This work was supported by the National Natural Science Foundation of China, Grant no. 42177270 and 42077218, the China Postdoctoral Science Foundation, grant no. 2021M700879, Guangdong Basic and Applied Basic Research Foundation, Grant no. 2021A1515110918.

AUTHOR CONTRIBUTIONS

LH, XL, YY, and SZ conceived and designed the study; LH performed the experiments, collected the data, and drew all figures. YY and XL wrote the manuscript; XL, YY, CR, SZ, and KN analyzed and interpreted the data; CR and KN revised the manuscript. All authors reviewed, revised, and approved the final manuscript.

COMPETING INTERESTS

The authors declare no competing interests.

ADDITIONAL INFORMATION

Supplementary information The online version contains supplementary material available at https://doi.org/10.1038/s41396-022-01335-3.

Correspondence and requests for materials should be addressed to Yong Yuan.

Reprints and permission information is available at http://www.nature.com/reprints

Publisher's note Springer Nature remains neutral with regard to jurisdictional claims in published maps and institutional affiliations.